ПРОГРЕСИВНІ ІНФОРМАЦІЙНІ ТЕХНОЛОГІЇ, ВИСОКОПРОДУКТИВНІ КОМП'ЮТЕРНІ СИСТЕМИ

UDC 519.004.942
DOI: 10.20535/SRIT.2308-8893.2021.1.01

SIMULATING ANGULAR MOMENTUM OF GRAVITATIONAL FIELD OF A ROTATING BLACK HOLE AND SPIN MOMENTUM OF GRAVITATIONAL WAVES

Y. MATSUKI, P.I. BIDYUK

Abstract. In this research, we simulated the angular momentum of gravitational field of a rotating black hole and the spin momentum of gravitational waves emitted from the black hole. At first, we calculated energy densities of the rotating gravitational field and spinning gravitational waves as the vectors, which were projected on the spherical curved surface of the gravitational field and of the gravitational waves. Then we calculated the angular momentum and the spin momentum as the vectors perpendicular to the curved surface. The earlier research by Paul Dirac, published in 1964, did not select the curved surface to calculate the motion of quantum particles; but, instead, he chose the flat surface to develop the theory of quantum mechanics. However, we pursued the simulation of the gravitational waves in spherical polar coordinates that form the spherical curved surface of the gravitational waves. As a result, we found that a set of anti-symmetric vectors described the vectors that were perpendicular to the spherical curved surface, and with these vectors we simulated the angular momentum of the rotating black hole's gravitational field and the spin momentum of gravitational waves. The obtained results describe the characteristics of the rotation of a black hole and of spinning gravitational waves.

Keywords: gravitational waves, angular momentum, curvature tensor, stress-energy tensor, black hole.introduction

INTRODUCTION

Research question

In our previous two researches [1, 2, 3], we reported that the antigravity and anti-gravitational waves appear when a black hole rotates, but we also reported that further research is needed to identify the vectors, which are pependicular to the rotating axis of the gravitational field and the gravitational waves. Then, in this new research, in order to further investigate this problem, we assumed as if the "$\sin\varphi$ component" to the rotational axis of φ represents the perpendicular direction of the curved surface described by spherical polar coordinates.

Theory of movement of the curved surface in the time-space coordinates

Dirac [4] explained two types of coordinate systems that describe time and space: one is in the flat space-like surface (Fig. 1), and another is the curved space-like surface (Fig. 2). In each figure three-dimensional surfaces (S_1, S_2, S_3, S_1' in Fig. 1

and S in Fig. 2) are placed in four-dimensional time-space, where x_0 is for time and x_1, x_2, x_3 are for the space. (Einstein's special theory of relativity is explained in Fig.1, while the general theory of relativity [5] is explained in Fig. 2) Dirac [4] described that Fig. 2 represents a three-dimensional curved surface in a four-dimensional space-time, which has the property of being everywhere space-like, and the normal (perpendicular) vector to the suruface must be in the light-cone in the Fig. 2. Dirac predicted that this perpendicular movement to the curved space must be physically meaningful.

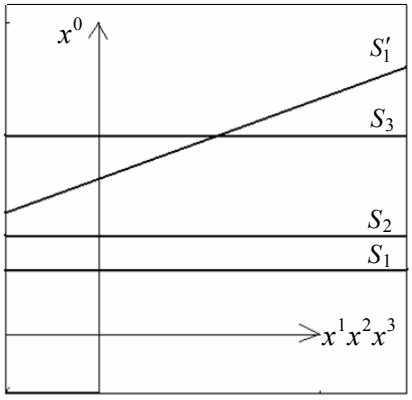

Fig. 1. Flat space-like surface (adapted from Reference [4])

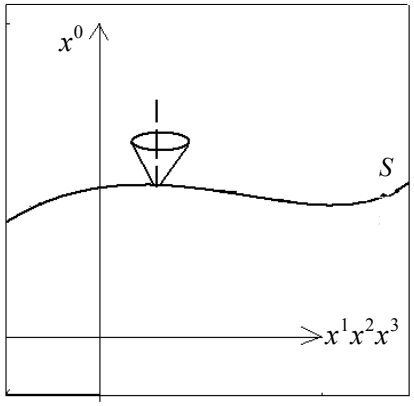

Fig. 2. Curved space like surface

In our research, we simulated the gravitational field and gravitational waves in the curved space-like surface using the spherical polar coordinate system so that we could still use the orthogonal transformation for modelling the rotation of a black hole. In our previous research [6], we simulated the energy density of the gravitational field and of the gravitational waves, also with the spin angular momentum of the gravitational waves on the flat surface; but, not the movements of the vectors perpendicular to the curved surface. In this article we report the result of our next research about the simulation of perpendicular component of the movement of the curvature tensors.

Curvature tensors

In this research, we used the same curvature tensors that we derived for our previous researches [2, 3], but we reorganized the components in the following formula for the gravitational field:

$$R_{\mu\nu} = \begin{bmatrix} R_{11} & 0 & 0 \\ 0 & R_{22} & 0 \\ 0 & 0 & R_{33} \end{bmatrix},$$

where $$R_{11} = \frac{20}{3(\rho-\tau)^2} + \frac{11\mu}{18m(\rho-\tau)^{4/3}};$$

$$R_{22} = \frac{28}{9\mu^2(\rho-\tau)^{10/3}} + \frac{140m}{9\mu^2(\rho-\tau)^4} + \frac{4}{\sin^2\theta} + \cot^2\theta,$$

and $$R_{33} = \frac{-28}{9\mu^2(\rho-\tau)^{10/3}\sin^2\theta} + \frac{140m}{9\mu^3(\rho-\tau)^4\sin^2\theta} + \frac{4}{\sin^2\theta} + \frac{11\cot^2\theta}{\sin^2\theta},$$

then we formulated the body vector of the black hole: $R = \begin{bmatrix} R_{11} & R_{22} & R_{33} \end{bmatrix}^{\mathrm{T}}$.

And for the simulation of the gravitational waves, we used the following formula, as three diagonal components of a 3×3 matrix:

$$\text{For } \varsigma = \eta = 1: \frac{-16}{9(\rho-\tau)^2} - \frac{2}{3(\rho-\tau)^2} - \frac{2\mu}{81m(\rho-\tau)^{10/3}} + \frac{\mu}{9m(\rho-\tau)^{7/3}} -$$

$$- \frac{\mu}{9m(\rho-\tau)^{4/3}} - \frac{2}{(\rho-\tau)^2} + \frac{224m}{9\mu^3(\rho-\tau)^4} + \frac{224m}{9\mu^3(\rho-\tau)^4 \sin^2\theta}.$$

$$\text{For } \varsigma = \eta = 2: \frac{24\cos\theta}{\sin^4\theta} + \frac{8}{\sin^2\theta}, \text{ and for } \varsigma = \eta = 3: \frac{64}{9(\rho-\tau)^2} - 32\cot^2\theta$$

and similarly we formulated the wave vector: $g = \begin{bmatrix} g_1 & g_2 & g_3 \end{bmatrix}^{\mathrm{T}}$.

The curvature tensors of gravitational waves, which penetrate the boundary of a black hole [2], are:

$$g^{\varsigma\eta}\rho_{\sigma,\varsigma\eta} + g^{\varsigma\eta}_{,\sigma}(g_{\rho\varsigma,\eta} - (1/2)g_{\varsigma\eta,\rho}) + g^{\varsigma\eta}_{,\rho}(g_{\sigma\varsigma,\eta} - (1/2)g_{\varsigma\eta,\sigma}) +$$

$$+ (1/2)g^{\rho\varsigma}g_{\beta\beta}g_{\rho\varsigma,\beta}g_{\eta\varsigma,\beta\sigma} + (1/2)g^{\rho\varsigma}g_{\beta\beta}g_{\rho\varsigma,\beta\sigma}g_{\eta\varsigma,\beta} + (1/2)g^{\rho\varsigma}_{,\sigma}g_{\beta\beta}g_{\rho\varsigma,\beta}g_{\eta\varsigma,\beta} +$$

$$+ (1/2)g^{\rho\varsigma}g_{\beta\beta,\sigma}g_{\rho\varsigma,\beta}g_{\eta\varsigma,\beta} + (1/2)g^{\sigma\varsigma}g_{\beta\beta}g_{\sigma\varsigma,\beta}g_{\varsigma\eta,\beta\rho} + (1/2)g^{\sigma\varsigma}g_{\beta\beta}g_{\sigma\varsigma,\beta\rho}g_{\varsigma\eta,\beta} +$$

$$+ (1/2)g^{\sigma\varsigma}_{,\rho}g_{\beta\beta}g_{\sigma\varsigma,\beta}g_{\eta\varsigma,\beta} + (1/2)g^{\sigma\varsigma}g_{\beta\beta,\rho}g_{\sigma\varsigma,\beta}g_{\eta\varsigma,\beta}.$$

Distortion of time and space in strong gravity

We used the same assumption of our previus research [3] for simulating the distortion of time and space, as shown in Fig. 3 and Fig. 4. In these figures, τ is a relative time in the coordinate system, which expands and shrinks depending on the distance r, where $\tau = t + f(r)$; and ρ is the relative distance, which expands and shrinks depending on the time t, where $\rho = t + g(r)$; and $f(r)$ and $g(r)$ are functions of r. For the simulation we assumed Case-1: $f(r) = \log r$; and $g(r) = e^r$ (non-linear); and Case-2: $f(r) = 1/r$, and $g(r) = r$ (linear).

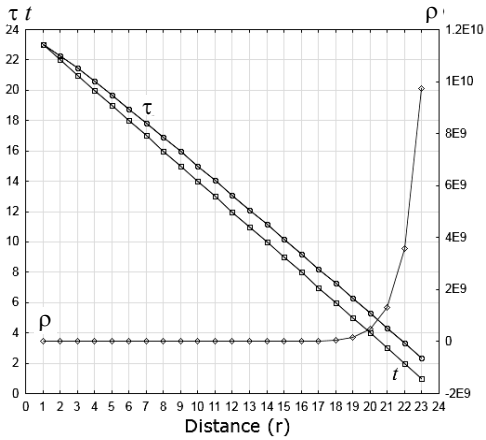

Fig. 3. Time and distance from the center of the gravitational field, Case-1 (non-linear distortion): $f(r) = \log r$ and $g(r) = e^r$

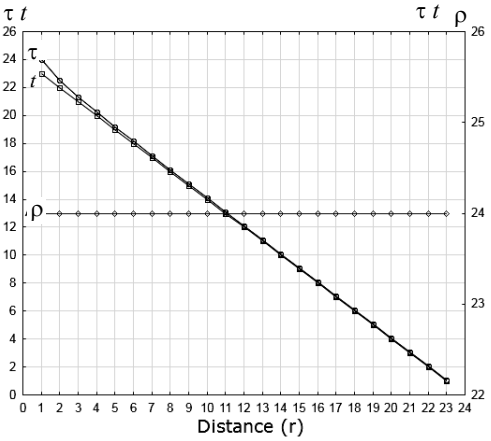

Fig. 4. Time and distance from the center of the gravitational field, Case-2 (linear distortion): $f(r) = (1/4)$ and $g(r) = r$

ALGORITHM

We used the same algorithm that we used for our previous research [3] to simulate the relative strengths (intensities) of the curvature tensors, which are reflected by the stress-energy tensor that is placed at the end of the distance r in Fig. 3 and Fig. 4.

Einstein's field equation [5] that rules the motion of particles in the gravitational field is as follows: $(R^{\mu\nu} - (1/2)g^{\mu\nu}R)_{,\nu} = 0$. Then $R_{\mu\nu} - (1/2)g_{\mu\nu}R = kT$, where T is the stress-energy tensor and k is a constant [7]. By calculating, c and $V(c)$, as shown below, we estimated the relative strength of each component of $R_{\mu\nu}$ to the stress-energy tensor in the system of spherical polar coordinates:

$$H = kT - R_{\mu\nu} = kT - (c_1X_1 + c_2X_2 + c_3X_3),$$

and

$$H^2 = \{kT - (c_1X_1 + c_2X_2 + c_3X_3)\}^2,$$

where c_1, c_2, and c_3 are the coefficients, which make a column vector c. And $X = [X_1 \quad X_2 \quad X_3]$, then $H = kT - Xc$. Then we set the constraint $X'H = 0$, then $X'(kT - Xc) = 0$, where X' is transpose matrix of X.

Then $X'Xc = X'kT$, $c = (X'X)^{-1}X'kT$ and $\Sigma = V(c) = \hat{\sigma}^2(X'X)^{-1}$, where $V(c) = \sigma^2$ is the variance of the c and $\hat{\sigma}^2 = e'e/(n-l)$, where $e = MkT$, $M = I - X(X'X)^{-1}X'$, n is the number of rows of each column of X (in this simulation $n = 23$), l is the number of columns of X, I is a 23×23 unit matrix that holds 1 on all diagonal elements and 0 for the other elements, $(X'X)^{-1}$ is the inverse matrix of $X'X$, and e' is the transpose vector of e.

Rotation of the black hole (an object), which contains strong gravity that distorts time and space

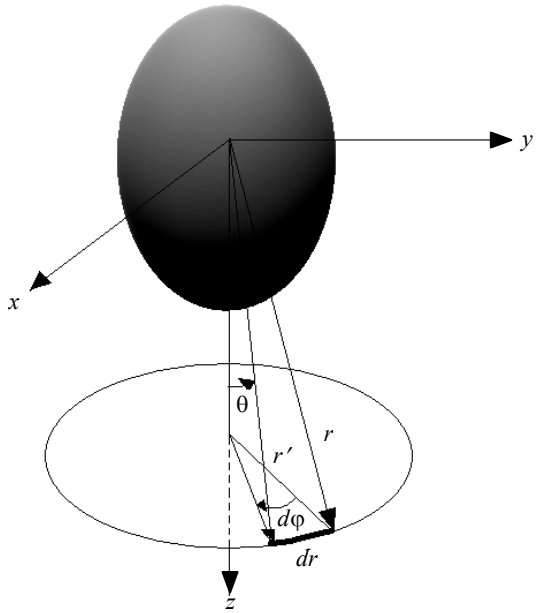

Fig. 5. Rotation of an object

When an object rotates as shown in Fig. 5, its coordinate system will be transformed by the transformation matrix D of the Euler's angles [7]. For the rotation around one axis of φ the tensors of the object's coordinate system will be multiplied by the matrix

$$D = \begin{bmatrix} \cos\varphi & \sin\varphi & 0 \\ -\sin\varphi & \cos\varphi & 0 \\ 0 & 0 & 1 \end{bmatrix}.$$

And then the curvature tensor $R_{\mu\nu}$ will be transformed to:

$$DR_{\mu\nu} = \begin{bmatrix} \cos\varphi & \sin\varphi & 0 \\ -\sin\varphi & \cos\varphi & 0 \\ 0 & 0 & 1 \end{bmatrix} \cdot \begin{bmatrix} R_{11} & 0 & 0 \\ 0 & R_{22} & 0 \\ 0 & 0 & R_{33} \end{bmatrix} = \begin{bmatrix} \cos\varphi \cdot R_{11} & \sin\varphi \cdot R_{22} & 0 \\ -\sin\varphi \cdot R_{11} & \cos\varphi \cdot R_{22} & 0 \\ 0 & 0 & R_{33} \end{bmatrix}.$$

Here the components $\sin\varphi \cdot R_{22}$ and $-\sin\varphi \cdot R_{11}$ are anti-symmetrical, which are perpendicular to the rotational axis $z = x_3$ for φ of Fig. 5.

Given the above transformed curvature tensor after the rotation, at first we calculated the relative strength of the principal moment of the rotation by the diagonal components of $DR_{\mu\nu}$, which are

$$\begin{bmatrix} dR_{11} & 0 & 0 \\ 0 & dR_{22} & 0 \\ 0 & 0 & R_{33} \end{bmatrix} = \begin{bmatrix} \cos\varphi \cdot R_{11} & 0 & 0 \\ 0 & \cos\varphi \cdot R_{22} & 0 \\ 0 & 0 & R_{33} \end{bmatrix}$$

to formulate $H = kT - (c_1 dR_{11} + c_2 dR_{22} + c_3 R_{33})$, then the algorithm follows as explained above.

And then we also calculated the anti-symmetrical components of $DR_{\mu\nu}$, which are

$$\begin{bmatrix} 0 & \sin\varphi \cdot R_{22} & 0 \\ -\sin\varphi \cdot R_{11} & 0 & 0 \\ 0 & 0 & 0 \end{bmatrix} = \begin{bmatrix} 0 & R_{22} d\Omega_3 & 0 \\ -R_{11} d\Omega_3 & 0 & 0 \\ 0 & 0 & 0 \end{bmatrix}$$

to calculate $\begin{bmatrix} dR_{11} \\ dR_{22} \\ dR_{33} \end{bmatrix} = \begin{bmatrix} R_{22} \cdot d\Omega_3 \\ -R_{11} \cdot d\Omega_3 \\ 0 \end{bmatrix}$ to formulate $H = kT - (c_1 \cdot R_{22} \cdot d\Omega_3 -$

$- c_2 \cdot R_{11} \cdot d\Omega_3)$, then the same algorithm follows as explained above.

Here, $\begin{bmatrix} 0 & d\Omega_3 & 0 \\ -d\Omega_3 & 0 & 0 \\ 0 & 0 & 0 \end{bmatrix} = \varepsilon$ is an infinitesimal rotation operator; while in general;

$\varepsilon = \begin{bmatrix} 0 & d\Omega_3 & -d\Omega_2 \\ -d\Omega_3 & 0 & d\Omega_1 \\ d\Omega_2 & -d\Omega_1 & 0 \end{bmatrix}$, according to Reference [7]; but in this our simulation $d\Omega_1 = d\Omega_2 = 0$, and $d\Omega_3 = \sin\varphi$. It calculates rotated vector as the cross-product of $R_{\mu\nu}$ and $d\Omega$,

$$\begin{bmatrix} dR_{11} \\ dR_{22} \\ dR_{33} \end{bmatrix} = R_{\nu\nu} d\Omega = \begin{bmatrix} R_{11} \\ R_{22} \\ R_{33} \end{bmatrix} \begin{bmatrix} d\Omega_1 \\ d\Omega_2 \\ d\Omega_3 \end{bmatrix} = \begin{bmatrix} R_{22} d\Omega_3 - R_{33} d\Omega_2 \\ R_{33} d\Omega_1 - R_{11} d\Omega_3 \\ R_{11} d\Omega_2 - R_{22} d\Omega_1 \end{bmatrix}.$$

For the simulation of gravitational waves, simply R_{11}, R_{22} and R_{33}, are replaced by the diagonal components of the gravitational waves, and henceforward, the same algorithm follows.

SIMULATION

Input data

Time t is set as shown in Fig. 3 for Case-1 and in Fig. 4 for Case-2, with which its slope to the distance r from the center of the gravitational field is a constant. For simulating the spatial expansion of the gravitational field we assumed, as if θ becomes larger in far distance. On the other hand, for simulating the flow of gravitational waves we assumed, that θ becomes smaller in far distance, as shown in Fig. 6. For simulating the rotation of the object we set two cases assuming φ_1 (the rotation1) and φ_2 (the rotation 2) also as shown in Fig. 6. With these settings $\sin\theta$, $\cos\theta$, $\cot\theta$ and $\cos\varphi$ behave like it is shown in Fig. 7.

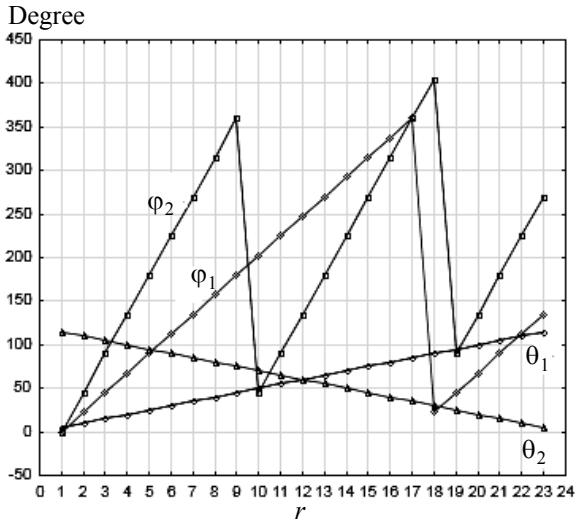

Fig. 6. Angles θ and φ for simulating gravitational field and gravitational waves

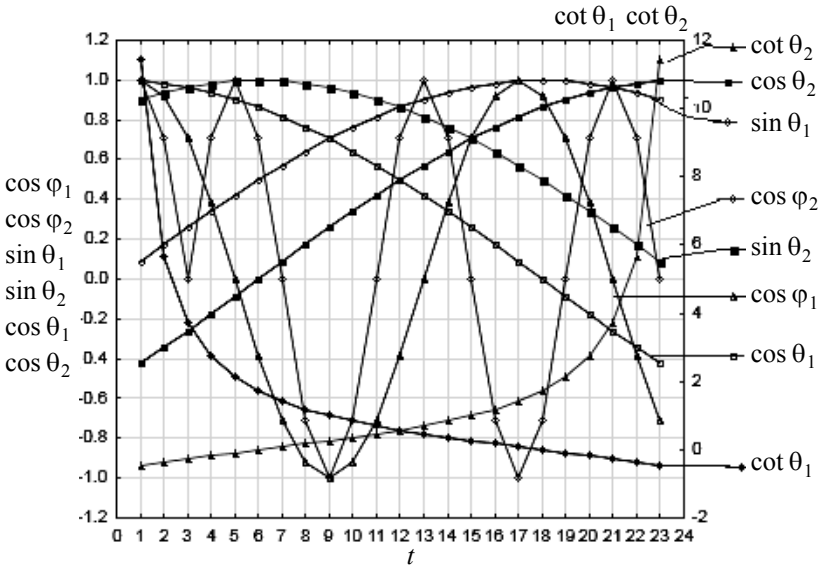

Fig. 7. $\mathrm{Sin}\theta$, $\cos\theta$, $\cot\theta$, and $\cos\varphi$ of the simulated gravitational field

In addition, for this simulation we set the stress-energy tensor $kT = 1$; because, the purpose of this simulation is to measure the order of magnitude of the relative strength of each component of $R_{\mu\nu}$ and the gravitational waves to the stress-energy tensor.

RESULT

Gravitational field

Fig. 8 (Table 1) shows the relative strengths of the gravitational field of the black hole, which are the gravitational field energy, projected on the spherical curved surface, and the angular momentum on the perpendicular vector to the surface, in Case-1 (non-linear distortion of the time and space) and Case-2 (linear distortion of time and space). As the rotation becomes more frequent from the rotation 1 to the rotation 2, the angular momentum (the perpendicular vector) changes from positive to negative. It means that the direction of the angular momentum changes, depending on the frequency of the rotation of the black hole. On the other hand, on the curved surface the gravitational field energy is negative (gravity) before the rotation in Case-1, but it changes to positive (antigravity) in the rotation 1, and then to negative (gravity) again in the rotation 2. It means that the antigravity appears, depending on the frequency of the rotation of the black hole. In Case-2, the gravitational field energy is positive (but smaller than in Case-1, and closer to zero) when the black hole doesn't rotate; while the gravitational field energy (negative) becomes larger when the black hole rotates faster. The angular momentum of Case-2 changes as it changes in Case-1.

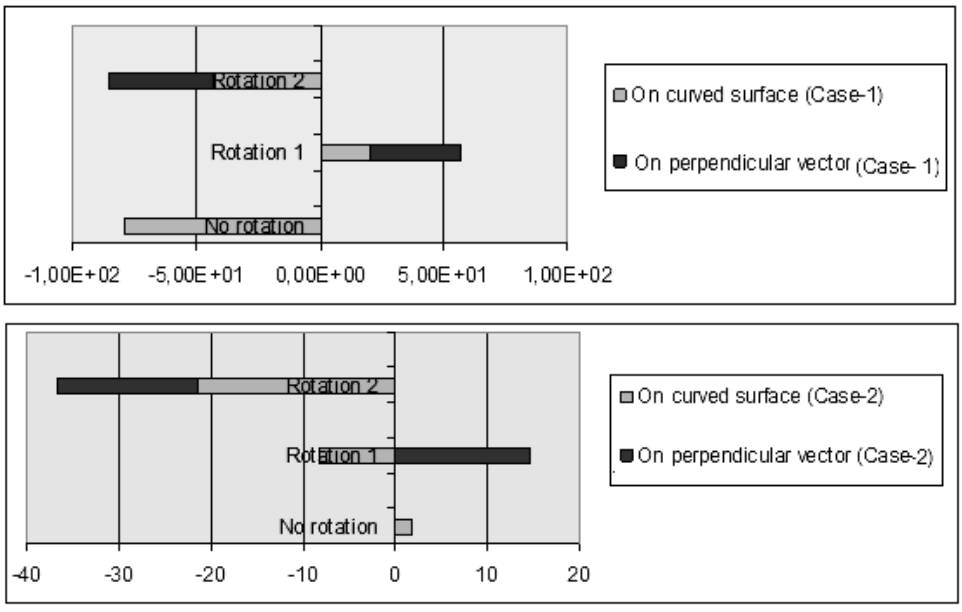

Fig. 8. Gravitational fields on curved surface and on perpendicular direction from the surface

Fig. 9 (Table 2) and Fig. 10 (Table 3) show the strengths of gravitational field energy, projected on the spherical curved surface in Case-1 and in Case-2, in

3 directions (projected on the spherical curved surface in the coordinates of r, θ, and φ, which are the generalized coordinates of $x_1 = x$, $x_2 = y$, and $x_3 = z$ of Cartesian coordinate system). In Case-1, only the r direction appears on the surface in all cases (no rotation, the rotation 1 and the rotation 2); while in Case-2, in addition to the direction of r, the component of θ appears as the black hole rotates.

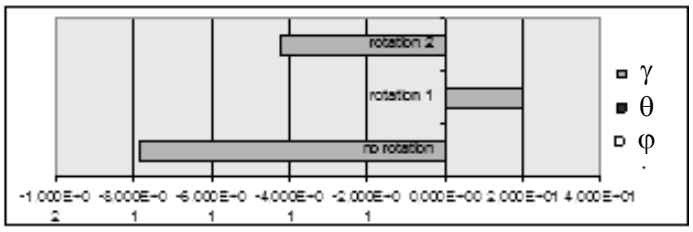

Fig. 9. Gravitational field energy in 3 directions on the spherical curved surface, Case-1

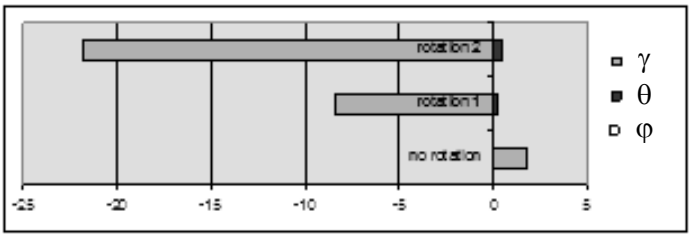

Fig. 10. Gravitational field energy in 3 directions on the spherical curved surface, Case-2

Fig. 11 (Table 4) and Fig. 12 (Table 5) show the strengths of the rotation's angular momentum in two directions (r and θ, which are perpendicular to the rotating axis, φ ($x_3 = z$ of Fig. 5)). Similar to the gravitational field energy, only the vector's component of r appears in Case-1; while the vector's component of θ also appears in Case-2. In both Case-1 and Case-2, as the frequency of the rotation increases from the rotation 1 to the rotation 2, the direction of the momentum changes from plus to minus. It suggests that the rotation of a black hole reverses its direction of the momentum when the frequency of the rotation changes.

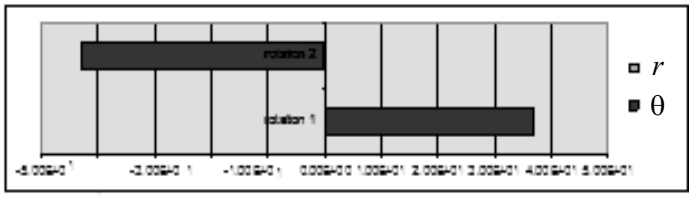

Fig. 11. Rotation momentum of the gravitational field in two directions of r and θ, Case-1

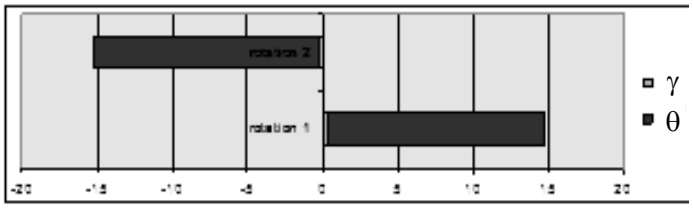

Fig. 12. Rotation momentum of the gravitational field in two directions of r and θ, Case-2

Gravitational waves

Fig 13 (Table 6) shows the srength of the gravitational waves emitted from the black hole, which are the energy (projected on the spherical curved surface of the wave) and the spin momentum of the rotation (projected on the pependicular direction to the surface), in Case-1 and Case-2. On spherical curved surface the energy of gravitational waves are not affected by the rotation; while on the perpendicular direction the rotational momentum (spin) appears, and it changes its direction from positive to negative when the frequency of the rotation changes from the rotation 1 to the rotation 2. It suggests, that the gravitationa waves make spin as the waves move on the direction of r as the emitter (the black hole) rotates, and it changes its spinning direction when the frequency of the rotation changes from the rotation 1 to the rotation 2.

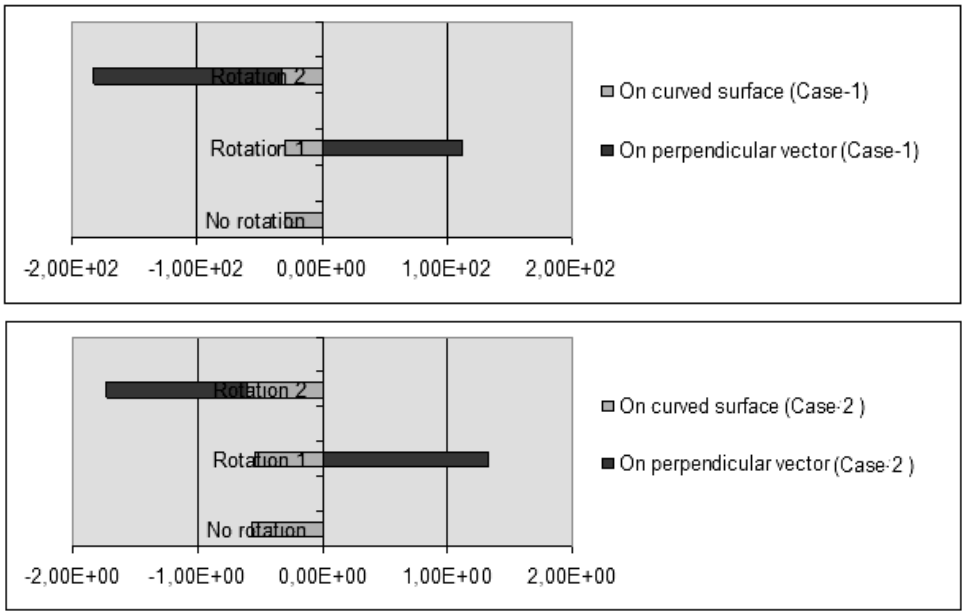

Fig. 13. Gravitational waves on curved surface and on perpendicular direction from the surface

Fig. 14 (Table 7) and Fig. 15 (Table 8) show the energy density of gravitational waves, projected on the spherical curved surface in three directions in Case-1 and Case-2. These figures suggest that the waves have negative energy density on the direction of r in Case-1; while the negative energy density appears also on the direction of rotation φ in Case-2. These figures suggest the appearance of anti-gravitational waves on the spherical curved surface. (The anti-gravitational waves must have negative sign [1], while gravitational waves must have positive sign). This finding is different from our previous report [3], in which either the gravitational waves or the anti-gravitational waves didn't appear when the black hole didn't rotate. The difference came from the configuration in the algorithm to formulate $H = kT - (c_1X_1 + c_2X_2 + c_3X_3)$. In this new research we reorganized the components of the curvature tensor into three vectors, X_1, X_2 and X_3; while in our previous report [3] we calculated the relative strength of every component of the curvature tensor by, $H = kT - (c_1X_1 + c_2X_2 + \cdots + c_nX_n)$.

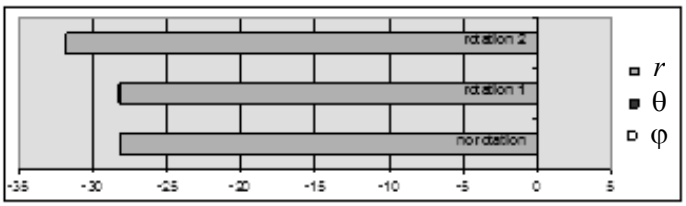

Fig. 14. Gravitational waves energy density on the curved surface, Case-1

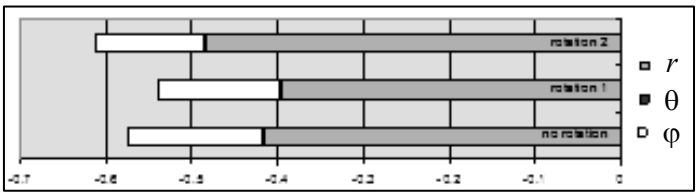

Fig. 15. Gravitational waves energy density on the curved surface, Case-2

Fig. 16 (Table 9) and Fig. 17 (Table 10) show the spin momentum of gravitational waves, projected in the directions of r and θ in Case-1 and Case-2. In

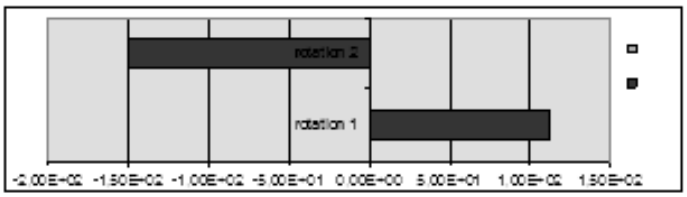

Fig. 16. Spin momentum of gravitational waves in two directions of r and θ, Case-1

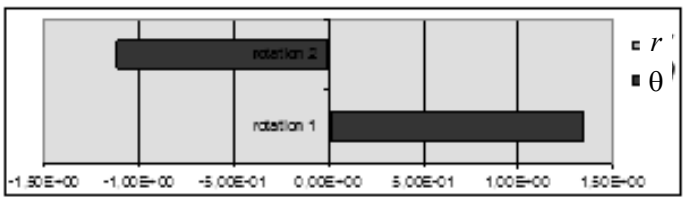

Fig. 17. Spin momentum of gravitational waves in two directions of r and θ, Case-2

both cases the vector component of θ appears in positive direction in the rotation 1, and in the negative direction in the rotation 2. These figures suggest that the gravitational waves changes its direction of spin as the rotation's speed of the black hole changes. its dsrection of spin as the rotation's speed of the black hole changes

PHYSICAL MEANING OF THE RESULTS

The components of $\cos\varphi$ in this analysis, which are the projections of the gravitational field and the gravitational waves on the spherical curved surface, are comparable to the vector component on the curved surface shown in Fig. 2 (at the beginning of this article). And the movements of these vectors are the movement of the curved surface itself. On the other hand, the vector components of $\sin\varphi$ are perpendicular to the curved surface, which is shown in the light-cone of Fig. 2, and the movement perpendicular to the curved surface must have real physical meaning. However, the earlier research by Paul Dirac [4] reported that it was problematic to quantize the movement of a quantum particle (gravitation is one of

them) such as calculating its momentum in the direction of the vectors, perpendicular to the curved surface. Henceforward, the theory of quantum mechanics was not developed on the curved surface (Fig. 2), but on the flat surface (Fig. 1).

In this research we simulated the gravitational waves on the surface of spherical polar coordinates as a surrogate of the general curved surface. And we used the cross product of anti-symmetrical vectors for simulating the components of $\sin\varphi$ as the mathematical model of the momentum in the light-cone of the general curved surface (Fig. 2).

CONCLUSIONS AND RECOMMENDATIONS

In this research we investigated the angular momentum of the gravitational field and the spin momentum of the gravitational waves by simulating the perpendicular component that is the "$\sin\varphi$ component" to the rotational axis of φ. We used the system of the spherical polar coordinates so that we could simulate the rotation with the orthogonal transformation of Euler's angles.

The result of the simulation shows that the rotating black hole can produce the antigravity and anti-gravitational waves; and the gravitational waves changes their spinning direction as the frequency of the black hole's rotation changes. These findings are consistent with our previous researches: [1] in which we reported that the negative flow of gravitational waves must have the clockwise spin, while the positive flow has the counter-clockwise spin; and [3] in which we reported that the antigravity and anti-gravitational waves appear when the black hole rotates.

In this research we used the system of spherical polar coordinates as the surrogate of the general curved surface; however, in near future, the developed computer technologies must increase a possibility of using general curved surface of Einstein's gravitational field equation also for solving the equation of motion of quantum particles.

Table 1. Strengths of gravitational field

Case	Case-1		Case-2	
	On curved surface	On perpendicular vector	On curved surface	On perpendicular vector
No rotation	-78,55	—	1,770	—
Rotation 1	20,00	36,90	-8,178	14,77
Rotation 2	-41,96	-43,00	-21,31	-15,29

Table 2. Strength of gravitational field on principal axis z, Case-1

Diagonal Components of $R_{\mu\nu}$	C and $\sqrt{V(c)}$ of $R_{\mu\nu}$ before the rotation	Diagonal Components of rotated $R_{\mu\nu}$	C and $\sqrt{V(c)}$ (Rotation 1)	C and $\sqrt{V(c)}$ (Rotation 2)
R_{11}	-78,68 (26,49)	$\cos\varphi \cdot R_{11}$	20,01 (58,22)	-42,05 (52,30)
R_{22}	0,1307 ($3{,}369 \cdot 10^{-2}$)	$\cos\varphi \cdot R_{22}$	$-5{,}516 \cdot 10^{-3}$ ($8{,}030 \cdot 10^{-2}$)	$8{,}903 \cdot 10^{-2}$ ($6{,}829 \cdot 10^{-2}$)
R_{33}	$-6{,}803 \cdot 10^{-5}$ ($2{,}557 \cdot 10^{-4}$)	R_{33}	$-3{,}290 \cdot 10^{-4}$ ($3{,}869 \cdot 10^{-4}$)	$-2{,}990 \cdot 10^{-4}$ ($5{,}403 \cdot 10^{-4}$)s
The values in the blackets are $\sqrt{V(c)}$				

Table 3. Strength of gravitational field on principal axis z, Case-2

Diagonal Components of $R_{\mu\nu}$	C and $\sqrt{V(c)}$ of $R_{\mu\nu}$ before the rotation	Diagonal Components of rotated $R_{\mu\nu}$	C and $\sqrt{V(c)}$ (Rotation 1)	C and $\sqrt{V(c)}$ (Rotation 2)
R_{11}	1,767 (7,364)	$\cos\varphi \cdot R_{11}$	-8,368 (11,85)	-21,79108 (16,36)
R_{22}	$2{,}862 \cdot 10^{-3}$ (0,1469)	$\cos\varphi \cdot R_{22}$	0,1924 (0,2427)	0,48490 (0,3369)
R_{33}	$1{,}110 \cdot 10^{-5}$ $(2{,}224 \cdot 10^{-3})$	R_{33}	$-2{,}854 \cdot 10^{-3}$ $(3{,}673 \cdot 10^{-3})$	$-7{,}281 \cdot 10^{-3}$ $(5{,}099 \cdot 10^{-3})$

Table 4. Strength of the perpendicular vector to the principal axis z of gravitational field, Case-1

Rotation	C and $\sqrt{V(c)}$ (Rotation 1)	C and $\sqrt{V(c)}$ (Rotation 2)
$dx_1 = R_{22} \cdot d\Omega_3 =$ $= \sin\varphi \cdot R_{22}$	$9{,}077 \cdot 10^{-2}$ $(5{,}072 \cdot 10^{-2})$	$-4{,}816 \cdot 10^{-2}$ $(5{,}931 \cdot 10^{-2})$
$dx_2 = -R_{11} \cdot d\Omega_3 =$ $= -\sin\varphi \cdot R_{11}$	36,83 (46,33)	-42,94 (45,44)

Table 5. Strength of the perpendicular vector of the rotating gravitational field, Case-2

Rotation	C and $\sqrt{V(c)}$ (Rotation 1)	C and $\sqrt{V(c)}$ (Rotation 2)
$dx_1 = R_{22} \cdot d\Omega_3 =$ $= \sin\varphi \cdot R_{22}$	0,28213 (0,2621)	-0,22852 (0,2597)
$dx_2 = -R_{11} \cdot d\Omega_3 =$ $= -\sin\varphi \cdot R_{11}$	14,48 (16,65)	-15,06 (16,69)

Table 6. Strengths of gravitational waves

Case	Case-1		Case-2	
	On curved surface	On perpendicular vector	On curved surface	On perpendicular vector
No rotation	-28,13	—	-0,5738	—
Rotation 1	-28,21	$1{,}125 \cdot 10^{2}$	-0,5396	1,341
Rotation 2	-31,84	$-1{,}505 \cdot 10^{2}$	-0,6123	-1,113

Table 7. Strength of gravitational waves, Case-1

Components of gravitational tensor	C and $\sqrt{V(c)}$ of $R_{\mu\nu}$ before the rotation	C and $\sqrt{V(c)}$ (After Rotation 1)	C and $\sqrt{V(c)}$ (After Rotation 2)
$x = x_1$ component	-28,06 (14,20)	-28,15 (15,52)	-31,84 (19,70)
$y = x_2$ component	$-4{,}594 \cdot 10^{-4}$ $(2{,}398 \cdot 10^{-4})$	$5{,}535 \cdot 10^{-4}$ $(2{,}987 \cdot 10^{-4})$	$1{,}167 \cdot 10^{-3}$ $(1{,}181 \cdot 10^{-3})$
$z = x_3$ component	$-6{,}855 \cdot 10^{-2}$ $(3{,}083 \cdot 10^{-2})$	$-5{,}955 \cdot 10^{-2}$ $(2{,}711 \cdot 10^{-2})$	$-8{,}950 \cdot 10^{-3}$ $(7{,}179 \cdot 10^{-3})$

Table 8. Strength of gravitational waves. Case-2

Components of gravitational tensor	***C* and $\sqrt{V(c)}$ of $R_{\mu\nu}$ before the rotation**	***C* and $\sqrt{V(c)}$ (After Rotation 1)**	***C* and $\sqrt{V(c)}$ (After Rotation 2)**
$x = x_1$ component	-0,4164 (0,2513)	-0,3967 (0,2734)	-0,4850 (0,3506)
$y = x_2$ component	$-1{,}116 \cdot 10^{-3}$ $(4{,}614 \cdot 10^{-4})$	$-1{,}009 \cdot 10^{-3}$ $(4{,}484 \cdot 10^{-4})$	$-8{,}918 \cdot 10^{-4}$ $(4{,}123 \cdot 10^{-4})$
$z = x_3$ component	-0,1562 $(6{,}097 \cdot 10^{-2})$	-0,1419 $(5{,}927 \cdot 10^{-2})$	-0,1264 $(5{,}444 \cdot 10^{-2})$

Table 9. Strength of the perpendicular vector to the principal axis z of gravitational waves. Case-1

Rotation	***C* and $\sqrt{V(c)}$ (Rotation 1)**	***C* and $\sqrt{V(c)}$ (Rotation 2)**
$dx_1 = R_{22} \cdot d\Omega_3 =$ $= \sin\varphi \cdot R_{22}$	$-9{,}438 \cdot 10^{-4}$ $(5{,}800 \cdot 10^{-3})$	$6{,}081 \cdot 10^{-3}$ $(3{,}813 \cdot 10^{-3})$
$dx_2 = -R_{11} \cdot d\Omega_3 =$ $= -\sin\varphi \cdot R_{11}$	$1{,}125 \cdot 10^{2}$ $(1{,}426 \cdot 10^{2})$	$-1{,}505 \cdot 10^{2}$ $(1{,}027 \cdot 10^{2})$

Table 10. Strength of the perpendicular vector of the rotating gravitational waves. Case-2

Rotation	***C* and $\sqrt{V(c)}$ (Rotation 1)**	***C* and $\sqrt{V(c)}$ (Rotation 2)**
$dx_1 = R_{22} \cdot d\Omega_3 =$ $= \sin\varphi \cdot R_{22}$	$1{,}025 \cdot 10^{-2}$ $(5{,}865 \cdot 10^{-3})$	$-5{,}437 \cdot 10^{-3}$ $(4{,}966 \cdot 10^{-3})$
$dx_2 = -R_{11} \cdot d\Omega_3 =$ $= -\sin\varphi \cdot R_{11}$	1,33031 (1,053)	-1,10749 (0,8583)

REFERENCES

1. Y. Matsuki and P.I. Bidyuk, "Analysis of negative flow of gravitational waves", *System Research & Information Technology*, no. 4, pp. 7–18, 2019.
2. Y. Matsuki and P.I. Bidyuk, "Numerical simulation of gravitational waves from a black hole, using curvature tensors, *System Research & Information Technology*, no. 1, pp. 54–67, 2020.
3. Y. Matsuki and P.I. Bidyuk, "Simulating the rotation of a black hole and antigravity", *System Research & Information Technology*, no. 3, pp. 124–137, 2020.
4. P.A.M. Dirac, *Lectures on quantum mechanics*; originally published by the Belfer Graduate School of Science. Yeshiva University, New York, 1964, 90 p.
5. P.A.M. Dirac, *General Theory of Relativity*. Florida University, A Wiley-Interscience Publication, John Wiley & Sons, New York, 1975, 70 p.
6. Y. Matsuki and P.I. Bidyuk, "Calculating energy density and spin momentum density of moon's gravitational waves in rectilinear coordinates", *System Research & Information Technology*, no. 3, pp. 7–17, 2019.
7. H. Goldstein, C.P. Poole, and J.L. Safko, *Classical Mechanics*. 3rd edition; published by Pearson Education Inc., 2002, 690 p.

Received 02.05.2020

INFORMATION ON THE ARTICLE

Petro I. Bidyuk, ORCID: 0000-0002-7421-3565, Educational and Scientific Complex "Institute for Applied System Analysis" of the National Technical University of Ukraine "Igor Sikorsky Kyiv Polytechnic Institute", Ukraine, e-mail: pbidyuke_00ukr.net

Yoshio Matsuki, ORCID: 0000-0002-5917-8263, National University of Kyiv-Mohyla Academy, Ukraine, e-mail: matsuki@wdc.org.ua

МОДЕЛЮВАННЯ КУТОВОГО МОМЕНТУ ГРАВІТАЦІЙНОГО ПОЛЯ ОБЕРТОВОЇ ЧОРНОЇ ДІРИ І СПІН-МОМЕНТУ ГРАВІТАЦІЙНИХ ХВИЛЬ / Й. Мацукі, П.І. Бідюк

Анотація. Змодельовано момент імпульсу гравітаційного поля обертової чорної діри і спін-моменту гравітаційних хвиль, що випромінюються з чорної діри. Спочатку обчислено питому енергію обертового гравітаційного поля і спін-моменту гравітаційних хвиль як векторів, що проєктуються на сферичну криволінійну поверхню гравітаційного поля та гравітаційних хвиль.Обчислено момент імпульсу та спін-момент як вектори, перпендикулярні до криволінійної поверхні. У своєму дослідженні, опублікованому в 1964 р., Поль Дірак обрав не криволінійну поверхню для обчислення руху квантових частинок, а плоску поверхню для розроблення теорії квантової механіки. У цій роботі зроблено спробу змоделювати гравітаційні хвилі у сферичних полярних координатах, які утворюють сферичну криволінійну поверхню гравітаційних хвиль. З'ясовано, що множина антисиметричних векторів описує вектори, перпендикулярні до сферичної криволінійної поверхні; з такими векторами змодельовано момент імпульсу гравітаційного поля обертової чорної діри і спін-момент гравітаційних хвиль. Отримані результати описують характеристики обертання чорної діри та обертання гравітаційних хвиль.

Ключові слова: гравітаційні хвилі, кутовий момент, тензор кривизни, тензор енергії напруження, чорна діра.

МОДЕЛИРОВАНИЕ УГЛОВОГО МОМЕНТА ГРАВИТАЦИОННОГО ПОЛЯ ВРАЩАЮЩЕЙСЯ ЧЕРНОЙ ДЫРЫ И СПИН-МОМЕНТА ГРАВИТАЦИОННЫХ ВОЛН / Й. Мацуки, П.И. Бидюк

Аннотация. Смоделирован момент импульса гравитационного поля вращающейся черной дыры и вращающего момента гравитационных волн, излучающихся из черной дыры. Сначала вычислена удельная энергия вращающегося гравитационного поля и вращающих гравитационных волн как векторов, проецирующихся на сферическую криволинейную поверхность гравитационного поля и гравитационных волн. Вычислены момент импульса и вращающий момент как векторы, перпендикулярные к криволинейной поверхности. В своем исследовании, опубликованном в 1964 г., Поль Дирак выбрал не криволинейную поверхность для вычисления движения квантовых частиц, а плоскую поверхность для разработки теории квантовой механики. В этой работе предпринята попытка смоделировать гравитационные волны в сферических полярных координатах, которые образуют сферическую криволинейную поверхность гравитационных волн. В результате выяснено, что множество антисимметричных векторов описывает векторы, перпендикулярные к сферической криволинейной поверхности; с такими векторами смоделированы момент импульса гравитационного поля вращающейся черной дыры и спин-момент гравитационных волн. Полученные результаты описывают характеристики вращения черной дыры и вращения гравитационных волн.

Ключевые слова: гравитационные волны, угловой момент, тензор кривизны, тензор энергии напряжения, черная дыра.